NORTHERN CALIFORNIA CHAPTER
AMERICAN ASSOCIATION *of* PHYSICISTS IN MEDICINE

Young Investigators Symposium
May 11, 2018: 10:30AM – 6PM
at the
Gladys Valley Hall **(Vet Med Instructional Facility)**
Room 2020
University of California at Davis, School of Veterinary Medicine

AGENDA

10:30AM Sign-In & Registration

11AM-NOON: Meet & Mingle at Lunch

NOON-12:45PM "Precision Imaging" (Keynote Address)
Martin G. Pomper, MD, PhD,
Henry N. Wagner, Jr. Professor of Pharmacology and Molecular Sciences at Johns Hopkins University, Baltimore, MD

1:00-2:00PM **PRESENTATIONS (Part I): *GRADUATE STUDENTS*:**

1. "Development of a focused X-ray luminescence tomography (FXLT) system" Michael C. Lun, Dept. of Bioengineering, School of Engineering, University of California, Merced
2. "Photodynamic therapy excited by high energy photons from Cesium 137 irradiator: *In vitro studies"*Yiping Guo, Quantitative and Systems Biology Program, School of Natural Sciences, University of California, Merced
3. "Magnetic Particle Imaging-Guided Heating in Vivo Using Gradient Fields for Arbitrary Localization of Magnetic Hyperthermia Therapy" Zhi Wei Tay, UC Berkeley
4. "Myocardial Creatine is Reduced in Obese Adults Despite Preserved Function: A Cardiac Chemical Exchange Saturation Transfer MRI Study". Wissam AlGhuraibawi. UC Berkeley

2:15PM 10 min BREAK/JUDGES CONFER

2:30-4:30 **PRESENTATIONS (Part II): *POST-DOCTORAL SCHOLARS*:**

5. "PET-Ball: A Closed Geometry Organ-PET for Small Animal Organs and Tissues", Levent Sensoy, PhD, Department of Biomedical Engineering, University of California, Davis
6. "Higher SNR PET Prediction using MRI and a Deep Learning Model", Chih-Chieh Liu, PhD, Department of Biomedical Engineering, University of California, Davis
7. "Imaging Bacterial Infection of the Heart with 6″-[18F]-Fluoromaltotriose PET/CT ", Dr. Mirwais Wardak, Department of Radiology & Stanford Cardiovascular Institute, Stanford University
8. "Development of the beta microscope for whole-tumor cellular-resolution imaging of PET tracers", Dr. Justin Klein, Stanford University

3:30PM – Refreshments arrive - 10 min Break?

9. "Digital Subtraction Angiography Magnetic Particle Imaging (DSA-MPI) and kinetic tracer modeling enabled gut bleed detection and quantitation in an in vivo murine model." Dr. Prashant Chandrasekharan, UC Berkeley
10. "Monte Carlo track-structure simulations with TOPAS-nBio", Jose Ramos-Méndez, UCSF

11. ""Neuroimaging of Inflammation by TSPO PET: Lessons from A Preclinical Model of Nerve Agent Exposure" Brad Hobson, PhD, Department of Biomedical Engineering, University of California, Davis

4:30-4:45M BREAK (JUDGES CONFER)

4:45-5:30PM **PRESENTATIONS (Part III): *MEDICAL PHYSICS RESIDENTS***

12. " Novel tungsten filled 3D Printed Electron Beam Shaping Devices: Design and Evaluation", Lawrie Skinner, PhD, Dept of Radiation Oncology, Stanford University
13. "Clinical Quality Assurance Applications of a High Spatial Resolution Diode Array for Small Field Dosimetry", Mareike Held, PhD, Radiation Oncology UCSF

5:30-6PM **SLAM COMPETITION (3 min presentations)**

6PM JUDGES CONFER

>6:00PM ANNOUNCEMENT OF AWARDS

TO FOLLOW TOUR UC Davis BME/PET EXPLORER

Tour of the Explorer Project – and overview of the development of whole body PET Imaging will be available after the Symposium.

Northern California Chapter of the AAPM – Young Investigators Symposium, May 11, 2018

ALL Presentation Titles and Abstracts

Johns Hopkins University

"Precision Imaging" (Keynote Address)

Martin G. Pomper, MD, PhD,
Henry N. Wagner, Jr. Professor of Pharmacology and Molecular Sciences at
Johns Hopkins University, Baltimore, MD

Approximately 20 years ago *in vivo* molecular imaging as a unique discipline coalesced around a variety of modalities used to answer specific biological questions. Now in the era of precision health imaging ascends to a new level of relevance. Precision medicine leverages individual differences in genetics, environment and lifestyle to provide optimum care. While precision medicine is primarily thought of in genetic terms, providing information about whether an individual may harbor disease, precision imaging makes precision medicine actionable by uncovering the location of where disease may be present – or may soon be manifested. As molecularly targeted and precise therapies are increasingly adopted, imaging agents must follow suit by being equally precise to be useful in guiding management. In some cases existing imaging techniques and agents may not be up to the task of guiding emerging cancer therapies, as with anatomic imaging (CT or MR) for cytostatic therapeutics or standard molecular imaging (FDG-PET) for immunotherapy. Theranostic agents enable imaging and therapy concurrently, or in rapid succession, and are often precisely targeted. An array of precision imaging agents and theranostics is coming online to manage patients in new ways. In addition to providing a brief overview of imaging biomarkers for precision medicine, we will discuss specific examples – including theranostics – that are in the process of or will soon be clinically implemented for targeting prostate cancer and for reporting on immunotherapies. An important aspect of this work is that the agents provide sensitive, specific and quantitative information.

Biography: Martin Pomper is the Henry N. Wagner, Jr. Professor of Radiology and Director of the Division of Nuclear Medicine and Molecular Imaging at Johns Hopkins Medical School. He received undergraduate, graduate (organic chemistry) and medical degrees from the University of Illinois at Urbana-Champaign. Postgraduate medical training was at Johns Hopkins, including internship on the Osler Medical Service, residencies in diagnostic radiology and nuclear medicine and a fellowship in neuroradiology. He is board-certified in diagnostic radiology and nuclear medicine. He has been on the Radiology faculty at Johns Hopkins since 1995, with several other joint appointments. His interests are in the development of new precision imaging agents for cancer, central nervous system disease and other disorders. He is a member of the National Academy of Inventors and the National Academy of Medicine.

UC Berkeley:

1. **“**Digital Subtraction Angiography Magnetic Particle Imaging (DSA-MPI) and kinetic tracer modeling enabled gut bleed detection and quantitation in an in vivo murine model.”
   Presenter Name: Dr. Prashant Chandrasekharan, Postdoc, UC Berkeley
   Abstract: Diagnosing gastrointestinal related bleeds quickly is indispensable for planning interventions. Scintigraphy techniques using 99Tcm-RBC is the most sensitive technique to date and relies on GMP process of labeling patient’s RBCs with radioisotopes of Tc99m prior diagnosis. The long preparatory time and exposure to radiation is a concern. In this study, we present a new imaging modality called Magnetic Particle Imaging (MPI) to detect GI Bleeds using long-circulating Superparamagnetic Iron Oxide nanoparticles (SPIO). Dynamic 2D projection MPI images were acquired over 120 minutes in a mouse model of intestinal bleed using PEG-coated SPIOs. The blood pool dynamic projection angiograms were processed by subtracting the first baseline blood pool image with the rest of the dynamic images. Digital subtraction angiography delineated and allowed accurate location of gastrointestinal bleeds. For quantitating the bleed rate, we first estimated the arterial blood input using a region-of-interest (ROI) approach over the ventricle of the heart. The MPI signal from the GI tract as a result of bleed was fit using a two-compartment tracer kinetic model. We used a non-linear least square based approach and a linear least square method (Patlak plot) to estimate the bleed rate. We estimated a bleed rate of 1 – 5 uL/min in our murine model. MPI was found to be ten times more sensitive in bleed detection when compared to scintigraphy technique. We believe that one-day MPI could be used in conjunction with CT or ultrasound for cases where bleeding has ceased, to complement the current clinical workflow for cases of occult or obscure GI bleeding. The robust contrast, sensitivity, safety, ability to image anywhere in the body, along with long-circulating SPIOs lends MPI outstanding promise as a clinical diagnostic tool for GI bleeding.

2. "Magnetic Particle Imaging-Guided Heating in Vivo Using Gradient Fields for Arbitrary Localization of Magnetic Hyperthermia Therapy”
   Presenter Name: Mr. Zhi Wei Tay, Graduate Student Researcher, UC Berkeley.
   Abstract: " Image-guided treatment of cancer enables physicians to localize and treat tumors with great precision. Here, we present in vivo results showing that an emerging imaging modality, magnetic particle imaging (MPI), can be combined with magnetic hyperthermia into an image-guided theranostic platform. MPI is a noninvasive 3D tomographic imaging method with high sensitivity and contrast, zero ionizing radiation, and is linearly quantitative at any depth with no view limitations. The same superparamagnetic iron oxide nanoparticle (SPIONs) tracers imaged in MPI can also be excited to generate heat for magnetic hyperthermia. In this study, we demonstrate a theranostic platform, with quantitative MPI image guidance for treatment planning and use of the MPI gradients for spatial localization of magnetic hyperthermia to arbitrarily selected regions. This addresses a key challenge of conventional magnetic hyperthermia. SPIONs delivered systemically accumulate in off -target organs (e.g. , liver and spleen), and difficulty in localizing hyperthermia results in collateral heat damage to these organs. Using a MPI magnetic hyperthermia workflow, we demonstrate image-guided spatial localization of hyperthermia to the tumor while minimizing collateral damage to the nearby liver (1− 2 cm distance). Localization of thermal damage and therapy was validated with luciferase activity and histological assessment. Apart from localizing thermal therapy, the technique presented here can also be extended to localize actuation of drug release and other biomechanical-based therapies. With high contrast and high sensitivity imaging combined with precise control and localization of the actuated therapy, MPI is a powerful platform for magnetic-based theranostics.

3. “Myocardial Creatine is Reduced in Obese Adults Despite Preserved Function: A Cardiac Chemical Exchange Saturation Transfer MRI Study”

Presenter Name: Mr. Wissam AlGhuraibawi, Graduate Student Researcher, UC Berkeley.
Introduction: Heart failure with preserved ejection fraction (HFpEF) is common in obese adults, yet little is known about corresponding changes in metabolic function. Compromised creatine (Cr) kinase system dynamics have been shown in HF with reduced EF using spectroscopy. Chemical exchange saturation transfer (CEST) – MRI enables imaging of tissue Cr levels with significantly higher sensitivity than spectroscopy. We previously demonstrated reduced Cr CEST contrast in obese mice with preserved systolic function. **Hypothesis**: We used CEST-MRI to test whether myocardial Cr CEST contrast is reduced in obese adults with preserved function compared to age matched healthy controls. **Method**: Obese (BMI>30, n=20) and healthy weighted (BMI<25, n=11) adults completed dual-energy x-ray absorptiometry to quantify body fat, and MRI. Left ventricular mass, volume, EF and global longitudinal strain (GLS) were calculated from a stack of short axis cine and four chamber cine images. CEST-MRI was performed in a mid-ventricular short axis slice with saturation offsets from -10ppm to 10ppm. Cr CEST contrast was calculated in the septum as MTR asym = (Signal $_{-1.8ppm}$ − Signal $_{1.8ppm}$)/Signal$_{-1.8ppm}$ × 100(%) after adjusting for field homogeneity. **Results**: EF (Obese 69 ± 9% vs Healthy 70 ± 4%, p = 0.95), GLS (Obese -24 ± 4% vs Healthy -22 ± 2%, p = 0.29), EDV (Obese 169 ± 52ml vs Healthy 148 ± 28ml, p = 0.17), ESV (Obese 52 ± 26ml vs Healthy 45 ± 10ml, p = 0.28), LVMI (Obese 62 ± 16g/m 2 vs Healthy 64 ± 15g/m 2 , p = 0.85) and Mass:Volume Ratio (MVR) (Obese 0.86 ± 0.16g/ml vs 0.75 ± Healthy 0.15g/ml, p = 0.1) were similar. While Cr CEST contrast was significantly reduced in obese adults (4.9 ± 4% vs 7.8 ± 2% Healthy, p = 0.01), there was no correlation with EF, LVMI, GLS, or MVR. **Conclusion**: CEST contrast generated by Creatine may represent a non-invasive sensitive marker of attenuated metabolic function in obese adults with preserved function.

UC Merced

4. **Photodynamic therapy excited by high energy photons from Cesium-137 irradiator: *In vitro studies***

Yiping Guo*, Shi Sheng†, Michael Lun‡, Wei Zhang‡, Shih-Ming Tsai‡, Wei-Chun Chin‡, Roy Hoglund§, and Changqing Li*‡
* Quantitative and Systems Biology Program, School of Natural Sciences, University of California, Merced, CA, USA 95343† Vascular Surgery, Union Hospital, Tongji Medical College, Huazhong University of Science and Technology, Wuhan, P.R. China, 430022‡ Department of Bioengineering, School of Engineering, University of California, Merced, CA, USA 95343§ Department of Animal Research Services, University of California, Merced, CA, USA 95343

Abstract
Photodynamic therapy (PDT) is a noninvasive cancer therapy method that has been clinically approved for many years. Due to the strong optical scattering and absorption of tissues, optical photons can only penetrate tissues in few millimeters which limit the applications of PDT to superficial lesions. To overcome the limitation of penetration depth, we used high-energy photons to excite photosensitizers directly to enhance PDT. A Cesium-137 irradiator has been used as the high-energy photon source and a fiber pigtailed diode laser was used to validate the efficacy of photosensitizer MPPa. A549 Human lung carcinoma cells were firstly treated with different concentrations of MPPa (10μM/mL, 5 μM/mL, 2.5 μM/mL, 1 μM/mL and 0 μM/mL) and then exposed to high energy photons for 30 min, 15 min, 7 min to 3 min, respectively. Moreover, to remove the possible plastic scintillation, we used both transparent and black 96-well plates in these studies. Our results indicated that high-energy photons enhanced PDT could potentially overcome the penetration limitations which makes PDT feasible for deep lesions.
Key words: Photodynamic therapy, high energy photons, Cesium-137 irradiator

5. **Development of a focused X-ray luminescence tomography (FXLT) system**
Michael C. Lun[1], Wei Zhang[1], Yue Zhao[1], Jeffrey Anker[2], Wenxiang Cong[3], Ge Wang[3], and Changqing Li[1,*]
Dept. of Bioengineering, School of Engineering, University of California, Merced (Merced, CA).
Dept. of Chemistry, Dept. of Bioengineering, Center for Optical Materials Science and Engineering Technology (COSMET) and Institute of Environmental Toxicology (Cu-ENTOX), Clemson University (Clemson, SC).
Dept. of Biomedical Engineering, Biomedical Imaging Center, Center for Biotechnology and Interdisciplinary Studies, Rensselaer Polytechnic Institute (Troy, NY).
Abstract:
Recently, X-ray luminescence computed tomography (XLCT) has emerged as a hybrid molecular imaging modality and has shown great promises in overcoming the optical scattering in deep tissues. However, its high spatial resolution capacity has not yet been fully implemented. In this talk, we will discuss our plans to build an XLCT imaging system, in which we will utilize a superfine focused X-ray beam to achieve an anticipated spatial resolution of 150 μm with high detection sensitivity for imaging deep targets in small-animals. After discussing the system design, we will demonstrate the feasibility of this system from different perspectives, including the spatial resolution, molecular sensitivity, and methods to improve the scan-time for the case of narrow/pencil beam XLCT imaging and then finally discuss some potential applications of the imaging system. The proposed Focused X-ray Luminescence Tomography (FXLT) imaging system will have potentials to help fill in the gap to provide the necessary high resolution and high-sensitivity imaging at depth.

Stanford University

6. **Title:** Development of the beta microscope for whole-tumor cellular-resolution imaging of PET tracers
Authors: Justin Klein, Tae Jin Kim, and Guillem Pratx
Abstract:
Molecular imaging of radiolabeled molecules has been crucial for understanding the fundamental machinery of cancer cells, for developing new therapies, and for monitoring therapy response. However, using positron-emission tomography (PET), it is possible only to study the aggregated behavior of millions of cells, complicating efforts to target aggressive cancers enabled by rare, yet insidious populations of progenitor cells.
Radioluminescence microscopy, an *in vitro* microscopy version of PET, was recently developed to address this need, and allows pharmacokinetic imaging of hundreds of cells simultaneously. However, the small field-of-view is insufficient for studying rare cell populations comprising <100 ppm.
We have developed a breakthrough modality, the *beta microscope*, for *in vitro*, cellularresolution PET tracer imaging of tumor-sized cell populations. The beta microscope can simultaneously image >100k cells, an 1,000X increase over state-of-the-art technology and has ~1 □m resolution, a 10X improvement over state-of-the-art technology. Additionally, the BM is a battery-powered, palm-sized device, capable of fitting into a standard incubator and costs <$50, ~100X less than RLM, its closest yet inferior equivalent. We have successfully used the beta microscope to image 18FDG in MDA-MB-231 breast cancer cells.
In this presentation we will report on the unique physics, performance characterization and latest advances in the development of the beta microscope. We will also discuss biological applications that will be enabled by this technological development.

Figure 1: 18FDG beta microscope image of MDA-MB-231 breast cancer cells. Grayscale image represents brightfield image. Overlayed heat map represents the beta signal from single cell 18FDG uptake.

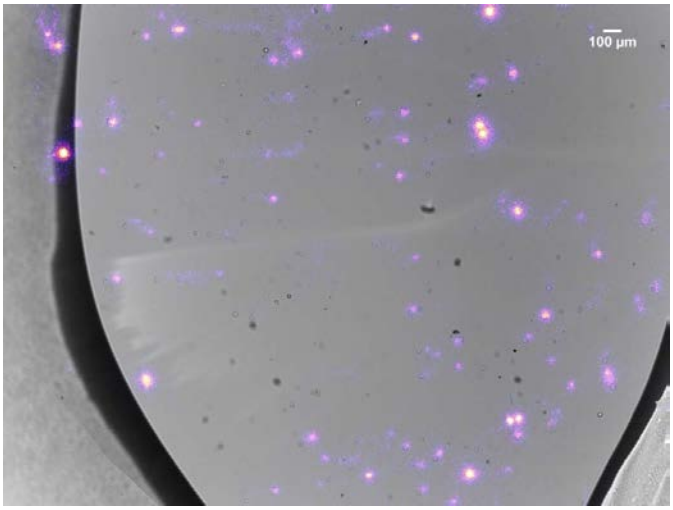

7. **Novel tungsten filled 3D Printed Electron Beam Shaping Devices: Design and Evaluation**
L Skinner, B Fahimian, A Yu.
Purpose: Two Cerrobend-free 3D printed solutions for electron field shaping are presented. The First solution, of 3D printed cutout trays offer more accurate field shaping, and improved safety by imprinting patient information into parts. While the second solution of a compact manual 3D printed electron MLC offers fast simulation to treat time. Both solutions remove toxic metals from the clinic and require less manual labor than current methods. **Methods:** Cutout tray shells, were designed and 3D printed. The workflow is streamlined by using a pre-designed blank tray template for each applicator size (6x6 up to 25x25) and merging it with the desired field outline. This shell is then filled with tungsten ball bearings. For the 3D printed MLC's designs were made to fit inside standard Varian electron applicators. The eMLC consists of 3D printed shells filled with tungsten powder. **Results:** The all-digital workflow of the 3D printed cutouts ensures accuracy and reproducibility. The dose difference between the aligned beam profiles of the 3D printed and Cerrobend cutouts was less than 1.2% at all measured points for 6MeV and 16MeV (ion chamber array measurements). The centering and accuracy of the 3D printed cut-outs was measured to be <0.5 mm. Whereas the Cerrobend cutout had 1-3 mm shift errors and 0.5-1.5 mm shape, compared to the plan. Transmission measurements through 3D printed, eMLC leaves show equivalent penumbra to Cerrobend parts.
Conclusion: Tungsten filled 3D printed cutouts were found to replicate the planned fields with improved alignment accuracy. Transmission and penumbra width were found to be equivalent to Cerrobend. The 3D printed static electron MLC designs allow for instant field shaping, without the wait for an electron cutout or CT simulation. These devices improve the accuracy and convenience of electron radiotherapy and open possibilities for novel, more precise electron treatments.

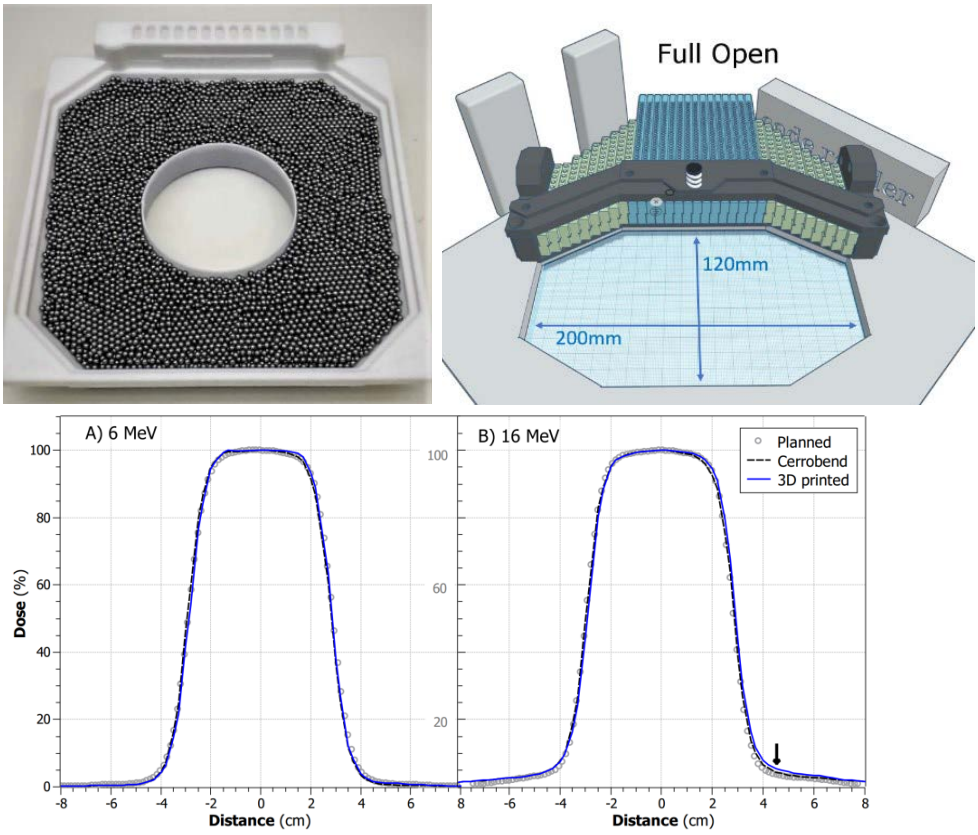

Fig. 1 TOP LEFT: 5.5 cm circle 3D printed cutout filled with tungsten ball bearings**. TOP RIGHT**: Preliminary design of 3D printable electron MLC. One half is shown for clarity. This design fits inside a standard Varian applicator, replacing the Cerrobend tray insert. This is for the large (25x25 cm2) electron applicator. A Scaled smaller version will be made to fit smaller applicators. **BOTTOM:** Crossline dose Profiles across 5.5 cm circular inserts measured at a 1.0 and 2.7 cm water equivalent depths for 6 and 16 MeV respective electron irradiations.

8. **Imaging Bacterial Infection of the Heart with 6′′-[^{18}F]-Fluoromaltotriose PET/CT** Authors: Mirwais Wardak[1,2], Gayatri Gowrishankar[1], Mohammad Namavari[1], Xin Zhao[2], Yonggang Liu[2], Tom Haywood[1], Evgenios Neofytou[2], Joseph C. Wu[1,2] and Sanjiv Sam Gambhir[1,2]
[1]Department of Radiology; [2]Stanford Cardiovascular Institute

Objectives: Infective endocarditis (IE) is a life-threatening disease with unacceptably high mortality rates. While imaging plays an important component of diagnosing IE, existing modalities are substantially limited. To address this problem, we have developed a novel positron emission tomography (PET) tracer 6′′-[^{18}F]Fluoromaltotriose, which is transported via the maltodextrin transporter, a transport system that is *exclusive* to bacteria and not present on mammalian cells. The purpose of this study was to investigate the diagnostic accuracy of 6′′-[^{18}F]Fluoromaltotriose PET/CT imaging in a preclinical bacteria-induced endocarditis model. **Methods:** 6′′-[^{18}F]Fluoromaltotriose uptake was evaluated in several clinically relevant bacterial strains in culture and in living mice. In the mouse endocarditis model, valve trauma was first induced by placing a 32G catheter at the aortic root via the right carotid artery. Bioluminescent *Staphylococcus aureus* bacteria (strain Xen 36; 10^6 CFUs) was then injected via tail vein 24h after surgery. Next, 6′′-[^{18}F]Fluoromaltotriose PET/CT imaging was performed 24h later for 60 minutes and quantitatively analyzed for tissue uptake and tracer kinetics. Lastly, animals were euthanized, and hearts and organs were removed and processed for biodistribution analysis and microbial assessment. **Results:** In-vitro cell uptake studies showed that 6′′-[^{18}F]Fluoromaltotriose was taken up by both Gram-positive and Gram-negative

strains of bacteria and not by mammalian cells. In the *Staphylococcus aureus*-induced infective endocarditis mouse model, there was an approximate 2.5-fold higher mean tracer uptake in the aortic valves of the infected mice (n=6) when compared to the control mice (n=6) (4.20 ± 1.06 %ID/g vs. 1.75 ± 0.41 %ID/g; $p<0.002$). Moreover, the signal on the PET images was confirmed by post-mortem examination. **Conclusions:** 6″-[^{18}F]Fluoromaltotriose was able to image valvular infection with high sensitivity and specificity. 6″-[^{18}F]Fluoromaltotriose promises to have significant diagnostic utility, with the potential to change the clinical management of patients suffering from infectious diseases of bacterial origin.

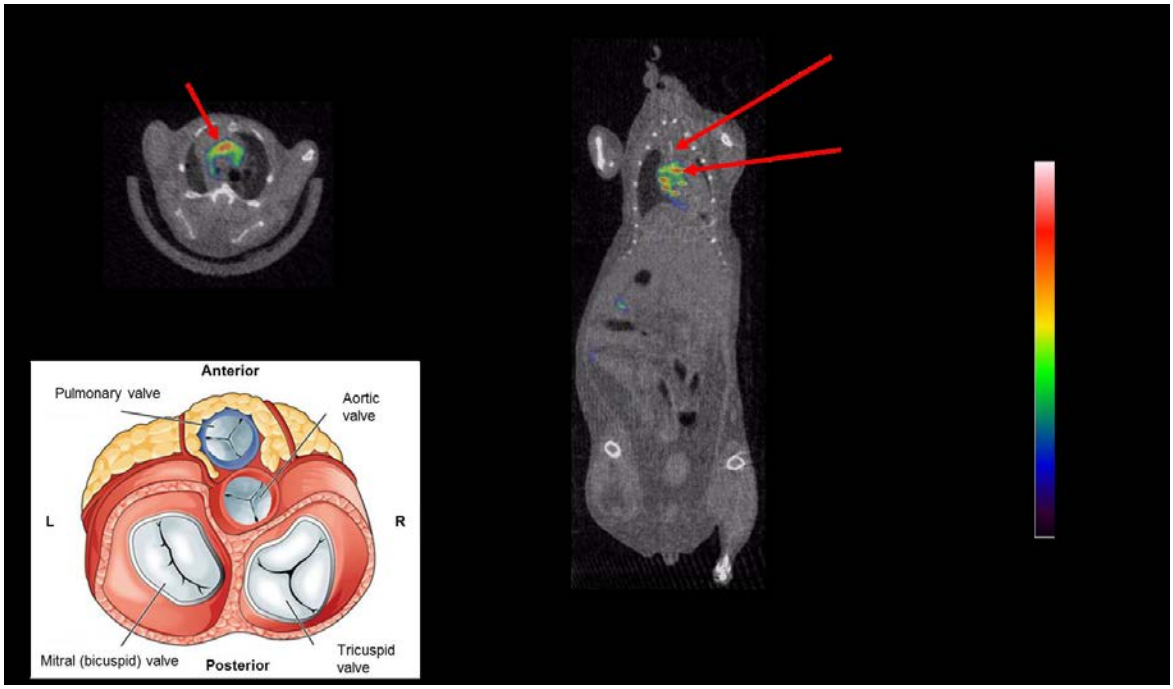

Figure 1. In the infective endocarditis mouse model, the heart had the highest PET signal above the diaphragm (as it was the source of infection). The kidneys had the highest signal below the diaphragm. Within the heart, the PET signal from the infected aortic valve had the highest tracer uptake and could be clearly seen; in some cases, the tricuspid valve was also infected (similar to what is seen for intravenous drug users).

UC Davis

9. Higher SNR PET Prediction using MRI and a Deep Learning Model

Chih-Chieh Liu1 and Jinyi Qi1
1Department of Biomedical Engineering, University of California, Davis, Davis, California

Abstract: Combining PET and MRI provides complementary morphologic and functional images, which could potentially improve PET image quality by many means. A common approach to improving PET image SNR based on deep learning requires training a deep neural network using higher SNR PET images as the label, which are not readily available. Here we propose a method with a U-Netbased deep neural network model to improve the SNR of PET images using MRI images without requiring any higher SNR PET images. Our proposed method provides an improvement of PET image SNR that is equivalent to a 1.7x increase in photon detection sensitivity and CNR that is 1.2x higher than that of ML-EM reconstruction.

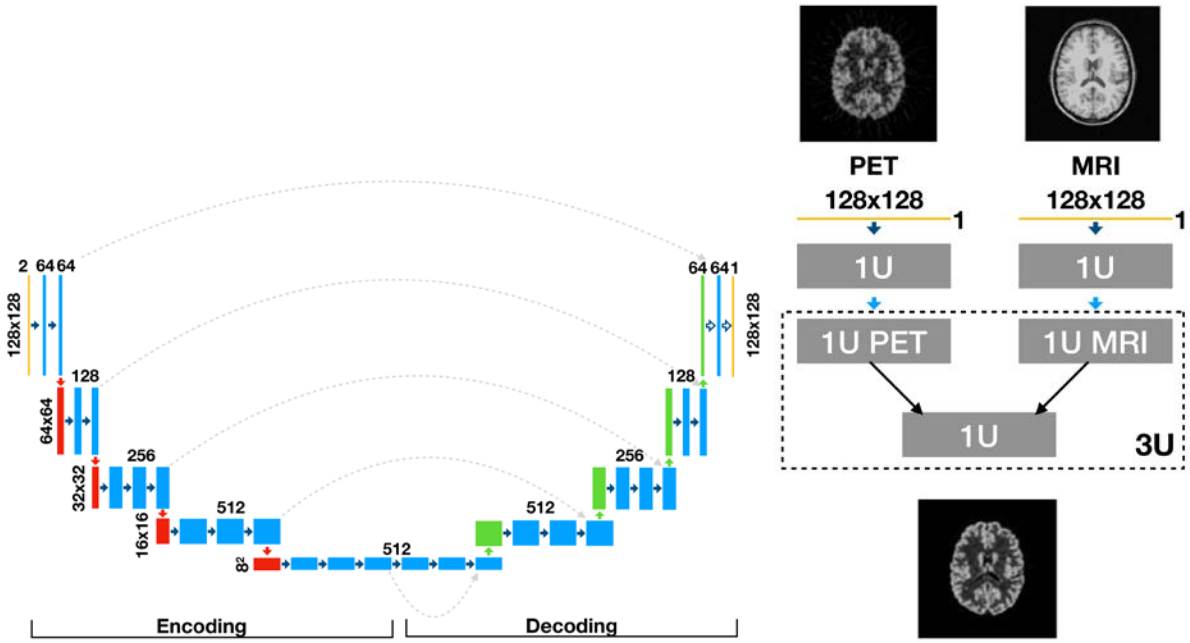

Figure 1: Proposed neural network model. Left: one U-Net architecture. Right: workflow of proposed there U-Net architecture.

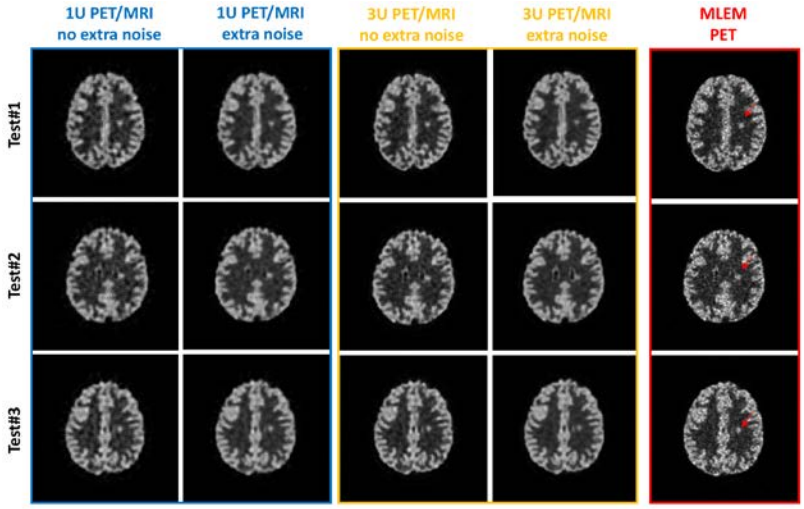

Figure 2: Inferences of three lesion test data. First two columns are 1U trained with PET/MRI without and with extra noise and the second two are 3U. The rightmost column is ML-EM reconstruction.

10. PET-Ball: A Closed Geometry Organ-PET for Small Animal Organs and Tissues

Levent Sensoy1***, Simon R. Cherry1
1Department of Biomedical Engineering, University of California, Davis, CA
*** Levent Sensoy is a Post-Doc at MiPET Research Group at UC Davis.

Abstract:

In small-animal Position Emission Tomography (PET), system sensitivity plays a more important role compared with human PET scanners in image quality as the total amount of emission from the small animal is much less than that from a human. Furthermore, the error introduced when determining lines of response (LOR) from detected gamma ray pairs that are radiated in coincidence from the source is less forgiving in a small-animal PET. In this study, we investigated sensitivity and scintillation position

identification accuracy of a novel prototype PET scanner designed specifically for imaging of excised murine tissue and organs. We aimed to demonstrate that a set of two monolithic hollow spherical scintillators, making a complete hollow sphere when coupled together, would be able to achieve 2-4 times better geometric efficiency in coincidence detection than existing state-of-the-art small-animal PET scanners by covering more than 95% of the solid angle. We also aimed to demonstrate that only a single layer of silicon photomultiplier (SIPM) arrays coupled on the outside of this scintillator would be sufficient to extract both angle and depth of the scintillation interactions within the scintillator, as opposed to other scanner geometries where dual-ended readouts or various forms of multi-layered scintillators are conventionally used to extract depth-of-interaction (DOI) information.

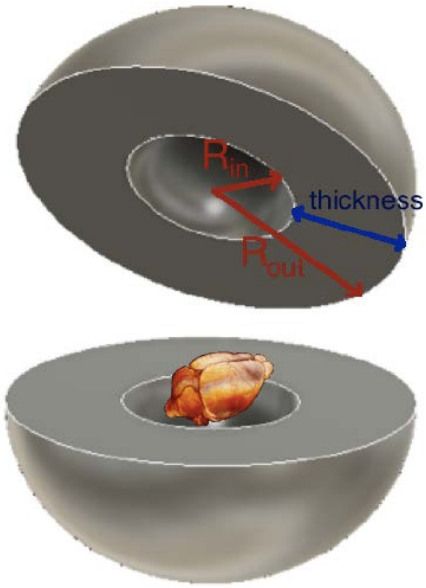

Figure. The geometric configuration of the monocrystalline scintillators of the proposed scanner. Inner radius (Rin) values ranging between 15 mm and 30 mm were studied. The outer radius (Rout) was kept as 35 mm in all cases. Thickness (i.e., (Rout) - (Rin)) is used as the identifier for different geometrical configurations. A rat brain can easily fit into the hollow space of the studied detector geometries.

11. **Title:** "Neuroimaging of Inflammation by TSPO PET: Lessons from A Preclinical Model of Nerve Agent Exposure" Brad A. Hobson[1], Douglas J. Rowland[1,2], Charlie Yu Ouyang[3], Donald A. Bruun[4], David L. Kukis[2], Daniel J. Tancredi[5], Simon R. Cherry[1,2,3], and Abhijit J. Chaudhari[2,3] Pamela J. Lein[4],
[1] Dept. of Radiology, UC Davis School of Medicine, Sacramento, CA, USA
[2] Center for Molecular & Genomic Imaging, Univ. of California, Davis, CA, USA
[3] Dept. of Biomedical Engineering, Univ. of California, Davis, CA, USA
[4] Dept. of Molecular Biosciences, Univ. of California, Davis, CA, USA
[5] Dept. of Pediatrics & Center for Healthcare Policy and Research, UC Davis School of Medicine, Sacramento, CA, USA

Purpose: The goal of this study was to evaluate PET imaging with the TSPO radioligand [^{18}F]PBR111 as a non-invasive tool for monitoring the spatiotemporal progression of neuroinflammation in a rat model of nerve agent intoxication using diisopropylfluorophosphate (DFP).
Methods and Materials: The validity of [^{18}F]PBR111-based TSPO PET imaging for the monitoring of neuroinflammation following acute DFP intoxication depends upon: 1) determining a rigorous method for quantifying binding of [^{18}F]PBR111 to TSPO in the brain, and 2) establishing that quantification of [^{18}F]PBR111 PET ultimately reflects the underlying neuropathology. First, we compared three kinetic models for radiotracer uptake: the reversible two-tissue compartment model (2T4k), simplified reference

tissue method using reference tissues based on cerebellum (SRTM-CB), and supervised cluster analysis with three kinetic classes (SRTM-SVCA3). We also measured the standardized uptake value (SUV). Second, we compared regional quantification of [^{18}F]PBR111 PET to gold standard histopathological assessment of inflammation at timepoints between 3 and 28 day post DFP intoxication.
Results: Model comparisons appeared to favor the reference tissue methods over 2T4k. Binding potential (BP_{ND}) estimates from SRTM-CB and SRTM-SVCA3 were correlated (R = 0.92, 95% CI [0.84, 0.96]), the latter having a smaller dynamic range and less sensitivity to longitudinal changes. The ratio of brain (excluding cerebellum) to cerebellum uptake (SUVR) was found to be highly correlated with BP_{ND} from SRTM-CB (R = 0.98, 95% CI: [0.97, 0.99]). DFP intoxication significantly increased [^{18}F]PBR111 SUVR within the hippocampus, thalamus, amygdala and piriform cortices ,which were in turn significantly correlated with histopathological assessment of neuroinflammation by glial fibrillary acidic protein (GFAP) (r_s = 0.65, 95% CI [0.38, 0.82]) and ionized calcium-binding adapter molecule 1 (IBA1) (r_s = 0.77, 95% CI [0.57, 0.89]) immunostaining.
Conclusion: Both SRTM-CB and SRTM-SVCA3 are viable alternatives to 2T4k, and with SUVR,may become potential endpoint for quantitative [^{18}F]PBR111 imaging in this model. PET imaging with the [^{18}F]PBR111 reflected underlying neuroinflammation following acute DFP intoxication; however, interpretation of these data is complicated by the multifaceted cellular biology underpinning PET imaging of TSPO.
Supported by NIH CounterACT program (NS079202).

UCSF

12. **Title:** Clinical Quality Assurance Applications of a High Spatial Resolution Diode Array for Small Field Dosimetry**Authors: Mareike Held, PhD**; Atchar Sudhyadhom, PhD Department of Radiation Oncology, University of California San Francisco.
Purpose: Stereotactic Radiosurgery (SRS) and Body Radiotherapy (SBRT) commonly utilize small field sizes for radiation delivery, and thus require high spatial resolution quality assurance (QA) devices. Diodes offer high spatial resolution but are also known to exhibit dependencies on field size, beam energy, dose rate, and incident beam angle, reducing dose measurement accuracy. The purpose of this study is to evaluate the dosimetric accuracy of a high spatial resolution diode array.**Methods:**A prototype of the SRSMC (SNC, Melbourne, FL) was used to evaluate and quantify its dependencies on field size (5mm to 80mm), beam energy (6MV WFF, 6MV FFF, and 10MV FFF), dose rate (repetition rates 100MU/min to 2400MU/min), and incident beam angle (0° to 90°). The SRSMC was calibrated on an Elekta VersaHD linac according to the vendor's instructions. Eight clinical VMAT treatment plans with energies of 6MV and 6MV FFF were measured with the SRSMC, for which it was placed inside SNC's StereoPHAN phantom and stereotactically positioned using the cone-beam CT on-board imaging system. The relative dose distribution was analyzed using the global gamma index with 3%/1mm criteria and dose difference index with 2% criteria. The absolute dose was evaluated in comparison to the measured dose using a PinPoint3D (PTW, Freiburg, Germany) ion chamber in a separate plan delivery. Software-based correction factors provided by SNC were evaluated for angular dependence, dose rate dependence, and temperature dependence correction.**Results:**The SRSMC has field size and beam energy dependencies for field sizes <2x2cm². Dose rate dependencies are >1% for dose rates <300 MU/min. Incident beam angle dependence is 2%. The software-based correction factors are applied effectively. The largest correction is made by accounting for the angular dependence. **Conclusion:** The

SRSMC is suitable for small field plan QA with some of the measured effects washing out on clinical plans. Plans with a majority of MUs delivered below 300MU/min and segment sizes <1x1cm² show larger errors when no correction is applied. The software-based corrections effectively account for the diode dependencies.

---

13. **Title**: Monte Carlo track-structure simulations with TOPAS-nBio.
Authors: Jose Ramos-Méndez and Bruce Faddegon Department of Radiation Oncology, University of California San Francisco.
Monte Carlo track-structure (MCTS) simulations extend, from first principles, the knowledge of the biological effects of radiation from microscopic to nanoscopic point-of-views. Through MCTS simulations, the spatial distribution of ionization events confined to a nanometer-scale region in space can be characterized, and biological outcomes such as DNA strand breaks can be simulated. In addition, Monte Carlo simulations are fundamental to design experimental setups and to assist in interpreting experimental data. Despite MCTS codes having been developed over the past 40 years, the access is generally restricted to the laboratories where they were developed. Aiming to extend the use of MCTS, the Geant4 Collaboration released in 2010 a prototype code through the Geant4-DNA project, highly attractive due to its open source availability. However, the use of Geant4 and Geant4-DNA involves a steep learning curve which limits the pool of users. To facilitate the development of simulations based on the physics of Geant4, a consortium financed by NCI/NIH and integrated by the University of California San Francisco, the Massachusetts General Hospital and the SLAC National Laboratory, developed the TOPAS Monte Carlo tool in 2012 to wrap and extend Geant4 for proton therapy applications. In the same way, to facilitate simulations based on Geant4-DNA, the TOPAS-nBio tool is under development. In this work, developments of chemical yield calculation implemented in TOPAS-nBio are presented with comparison to published experimental data. Simulations cover the three stages of radiation transport included in radiolysis; that is, the physical, physico-chemical and non-homogenous chemical stages. Optimization techniques implemented in TOPAS-nBio and limitations of the physico-chemical models available in Geant4-DNA are discussed.

---

14. **Title** : DoseNet: A Volumetric Dose Prediction Algorithm Using 3D Fully-Convolutional Neural Networks
Authors Vasant Kearney, Jason W. Chan, Samuel Haaf, Martina Descovich, Timothy D. Solberg
Purpose: Convolutional neural network (CNN) based dose prediction has been successful in predicting radiotherapy doses on 2D planes based on simple IMRT co-planar plans. However, the perceptive fields of such approaches are limited to 2 dimensions, which render them disadvantaged when handling non-coplanar dose predictions. To mitigate this, the present study suggests a novel deep learning volumetric non-coplanar dose prediction model that utilizes a novel 3D fully-convolutional neural network

architecture. **Methods**: This study evaluates the root mean squared error (RMSE), and common clinical dosimetric criteria differences between clinically approved dose (CAD) and a stacked fully-connected network (FC), a 2D CNN (2D-CNN), and a 3D CNN (DoseNet). This study considers 146 SBRT prostate patients treated using non-coplanar plans on a CyberKnife machine. Volumetric dose is predicted based on the planning CT, prostate, urethra, bladder, rectum, and penile bulb. The network accepts each input independently, creating interdependent hierarchical relationships between the structures and the planning CT, which allows the network to consider tissue inhomogeneity and structural geometries simultaneously.**Results**: DoseNet achieved superior dosimetric congruence with the clinically approved dose than FC and 2D CNN for the Dmax, Dmean, D95, and D99 of the PTV. DoseNet also predicted more dosimetrically similar organ at risk maximum values, for the rectum, penile bulb, urethra, and bladder. DoseNet required 600 epochs to train, which took ~14 hours on two Nvidia 1080 Ti graphics processing units (GPU)s. DoseNet makes a full volumetric prediction in ~1 second. **Conclusions**: This study has demonstrated that 3D fully-convolutional neural networks are capable of achieving superior dosimetric prediction accuracy than fully-connected networks and 2D based CNNs. Highest dosimetric improvement was seen in high dose regions.